ACS APPLIED MATERIALS & INTERFACES

Research Article

www.acsami.org

Electrorheological Operation of Low-/High-Permittivity Core/Shell SiO_2/Au Nanoparticle Microspheres for Display Media

Chung-Lin Li,[†] Jem-Kun Chen,*[,†] Shih-Kang Fan,[‡] Fu-Hsiang Ko,[‡] and Feng-Chih Chang[‡]

[†]Department of Materials and Science Engineering, National Taiwan University of Science and Technology, 43, Sec. 4, Keelung Road, Taipei, 106, Taiwan, Republic of China

[‡]Department of Applied Chemistry, Materials and Science Engineering, National Chiao Tung University, 1001, University Road, Hsinchu, 300, Taiwan, Republic of China

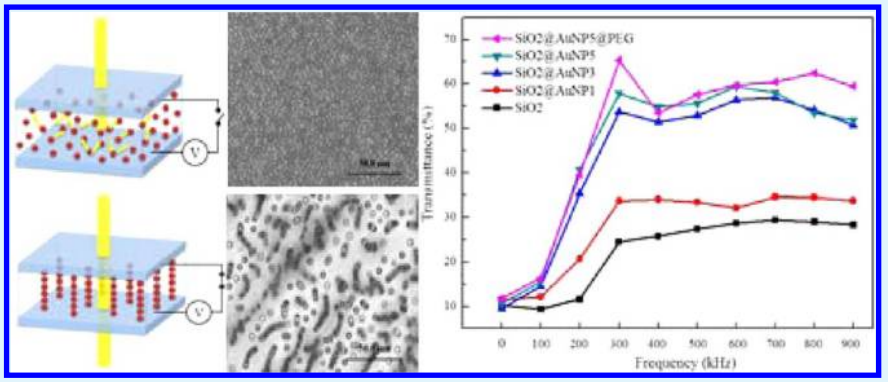

ABSTRACT: In this study, we synthesized core/shell structures comprising monodisperse 3-μm SiO_2 microspheres and gold nanoparticles (AuNPs, ca. 6.7 nm) as the core and shell components, respectively. Using a layer-by-layer cross-linking process with a dithiol cross-linking agent, we prepared low-permittivity AuNP-encapsulated high-permittivity SiO_2 core/shell microspheres with variable AuNP shell thicknesses. The dispersivity of the microspheres in solution was enhanced after grafting poly(ethylene glycol) monomethyl ether thiol (PEG-SH) onto the AuNP layer on the SiO_2 microspheres. Transmission electron microscopy (TEM) and scanning electron microscopy (SEM) images revealed sesame ball-like structures for these SiO_2@AuNP@PEG microspheres. We encapsulated aqueous dispersions of these SiO_2@AuNP microspheres into sandwich structured displays (SSDs) to investigate their electrorheological properties, observing reversibly electroresponsive transmittance that is ideally suited for display applications. Increasing the thickness of the AuNP layer dramatically enhanced the stringing behavior of the SiO_2 microspheres, resulting in increased transmittance of the SSD. The response time of the electroresponsive electrorheological fluids also decreased significantly after modifying the SiO_2 with the AuNP layers. The effective permittivities of these composites could be predicted from the real ($\acute{\varepsilon}$) and imaginary ($\acute{\varepsilon}$) parts of the Clausius−Mossotti formalism.

KEYWORDS: *core/shell, gold nanoparticle, SiO_2 microsphere, electrorheology*

INTRODUCTION

Electronic paper (e-paper) is an attractive material for visual display terminals because of its high reusability and flexibility, low power consumption, and lightweight.[1,2] In recent years, many techniques have been developed to realize electronic paper, which combines the desirable viewing characteristics of conventional printed paper with the ability to manipulate the displayed information electronically; such displays include Gyricon displays,[3] electrowetting displays,[4] liquid crystal reflective displays,[5] and electrophoresis displays.[6]

An electronic paper based on the electrophoretic motion of suspended light-scattering particles in a dielectric fluid when a voltage is applied has been realized by encapsulating the electrophoretic suspension into individual microcapsules or vessels.[7] Among the developed electronic paper display technologies, particle-based systems exhibit excellent performance by displaying the color of the dyed particles. Building an external electric field inside a particle suspension leads to charge/ion accumulation where the conductivity and permittivity feature discontinuities. If the particles in suspension are polarized, they would be attracted or repelled by the electric field resulting from field−dipole interactions, a phenomenon known as dielectrophoresis.[4,8] Electroresponsive electrorheological (ER) fluids comprising electrically polarizable particles (dimensions: 1−100 μm; volume fraction: 0.05−0.5) dispersed in insulating oils (e.g., mineral oil, silicone) exhibit fascinating field-induced rheological properties, including rapid and reversible changes in suspension microstructures under applied electric field strengths of up to several kilovolts per millimeter.[9] In studies of traditional ER fluids, polarized particle chains can

Received: August 8, 2012
Accepted: September 27, 2012
Published: September 27, 2012

Scheme 1. Schematic Representation of the Preparation of SiO_2@AuNP@PEG Core/Shell Composite Microspheres

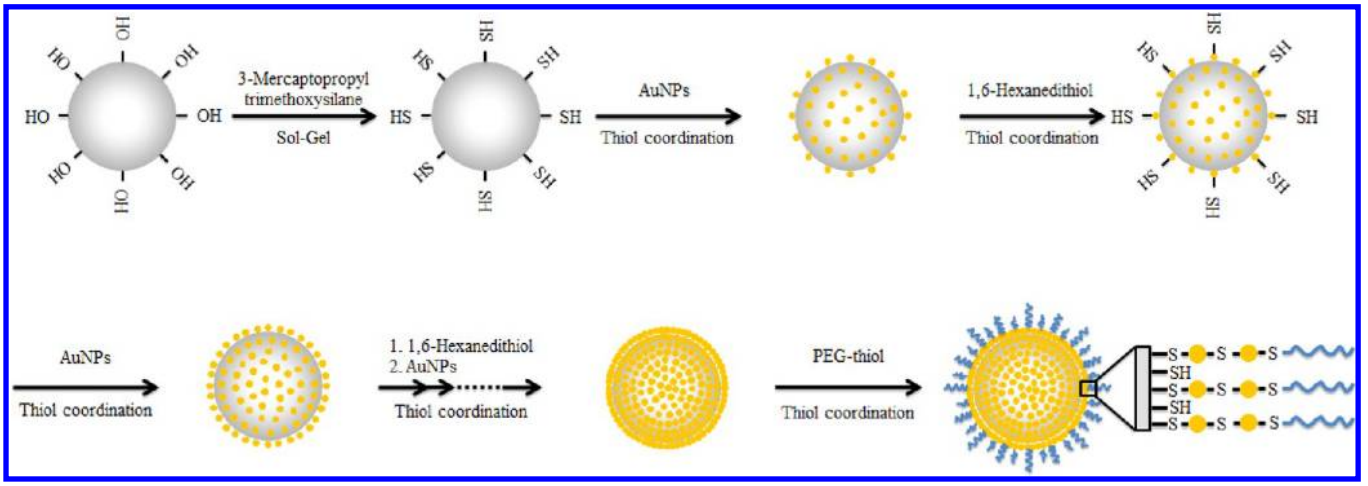

be applied to modulate the direction-dependent shear modulus of the particle suspensions.[10]

Core/shell materials consist of a core structural area covered by a shell area. The core and shell areas may be composed of a variety of materials, including polymers, inorganic solids, and metals.[11] Core/shell materials are typically spherical, but other shapes are possible. In the past decade, silica/metal particles comprising a silica core and a nanostructured metal shell have attracted much attention because of their potential applications in biosensors[12] and electronics[13] and to enhance the luminescence properties of particles.[14] The resulting composite particles are known as core/shell nanostructures, because the cores of these particles are large nonporous silica spheres and the shells are composed of metal nanoparticles (NPs). Among the various core/shell materials that have been developed, silica/metal particles are very popular and have been studied extensively.[15] Several approaches have been developed for the deposition of metal particles onto dielectric cores, including thermal evaporation techniques and seed methods,[16] electroless plating,[17] in situ chemical reduction,[18] self-assembly,[19] and sol–gel methods.[20] Almost all of these techniques result in low or nonuniform particle densities in the shell area. The shell density can be affected by the strength of attraction between the core and shell particles and also by the balance of attractive and repulsive forces between the particles in the shell area.[21] Organic linkers presenting surface thiol groups can be prepared from the silica particles through postsynthesis reactions with residual Si–OH groups[22] or through direct synthesis based on co-condensation of silica precursors with alkoxysilanes.[23] As a result of these surface modification processes, thiol-functionalized silica particles have found applications.[24]

Metallic atomic clusters—metal atomic aggregates of less than approximately 50–100 atoms (size: <1.5 nm), such as gold nanoparticles (AuNPs)—are interesting because they can exhibit novel properties.[25,26] Whereas a single AuNP could be regarded as an insulator, bulk Au is an excellent conductor; therefore, the conductivity of Au clusters can be adjusted by varying the degree of aggregation through interactions with dithiol groups.[27] In addition, it is expected that materials having high dielectric permittivity, high breakdown strength, low loss, and rapid response will be essential components in next-generation electrical and electronic applications. Conventional ceramic dielectrics, such as silica particles, have high permittivities and low working voltages. Core/shell-type SiO_2/Au clusters of the general structure provide a convenient medium to study the influence of the bonding on the properties of NP aggregates. These clusters consist of AuNPs that are attached to the surfaces of submicrometer SiO_2 spheres through organic linkers. Groups with various linkage capabilities are readily introduced on the surfaces of silica particles by means of organosilanes[28] and on the surfaces of AuNPs by means of thiols.[29] Aggregated Au clusters possessing low permittivity significantly contrast with SiO_2 microspheres, resulting in a large disparity in electric fields within the constituent phases, thereby inducing discontinuous variations in the local electric field at the interfaces and adversely affecting the bulk dielectric properties. In this study, we prepared core/shell-type SiO_2@AuNP microspheres by attaching layers of AuNPs onto the surfaces of SiO_2 microspheres through a layer-by-layer approach with a dithiol agent, forming poly(AuNP), and then investigated their electrorheological properties.[30] The monodisperse AuNPs cross-linked in a layer-by-layer manner in the form of poly(AuNP) exhibited variations in their permittivity because of the transition from insulator to semiconductor forms of the AuNPs.[30] In addition, we grafted a thiol-terminated polymer onto the poly(AuNP) surface to enhance the dispersivity of the core/shell microspheres and then fabricated a sandwich structured display (SSD) to encapsulate these aqueous suspensions. Upon applying an electric field to the SSD, these microspheres were strung linearly along the electric field at various frequencies, resulting in significant changes in transmittance. Using this approach makes it possible to create aqueous suspensions of microspheres that are ideally suited for display applications and, if desired, may be cycled between transparent and opaque states.

EXPERIMENTAL SECTION

Materials. SiO_2 microspheres (size: ca. 3 μm) were purchased from Polysciences; hydrogen tetrachloroaurate(III) trihydrate ($HAuCl_4 \cdot 3H_2O$, 99.9%), tetra-*n*-octylammonium bromide (TOAB, $C_{32}H_{38}BrN$, 98%), and sodium borohydride ($NaBH_4$, 98%) were purchased from Acros Organics. Poly(ethylene glycol) monomethyl ether thiol (PEG-SH; molecular weight: 5000 g/mol) and all other chemicals were purchased from Sigma-Aldrich in reagent grade; all solvents were of reagent grade and used without further purification. The immobilizers 1,6-hexanedithiol and (3-mercaptopropyl)-trimethoxysilane (MPTMS) were purified through vacuum distillation prior to use. The SU-8 (2000 series, MicroChem), stainless-steel spacer (1.5 × 1.5 cm; thickness: 100 μm; MiSUMi), Teflon (AF1600,

dx.doi.org/10.1021/am301543h | ACS Appl. Mater. Interfaces 2012, 4, 5650–5661

DuPont), and indium tin oxide (ITO) glass plates (5 × 5 cm^2; Delta Technologies) were used to fabricate the SSDs.

Layer-by-Layer Assembly of AuNPs onto SiO_2 Microspheres (SiO_2@AuNP). To allow surface reactions to occur during the metal nucleation and growth processes, the AuNPs were grown in a two-phase system.[22,31] In a typical synthesis, an aqueous solution of $HAuCl_4$ (0.35 wt %) was mixed with a solution of TOAB (0.687 g) in toluene (120 mL) for 30 min. A freshly prepared aqueous solution of $NaBH_4$ (0.32 wt %) was added slowly with vigorous stirring. This solution of AuNPs was used throughout all experiments. After being stirred for 6 h, the organic phase was separated, concentrated (to 20 mL) in a rotary evaporator, and mixed with EtOH (800 mL) to remove excess thiols. The colloidal solutions obtained were very stable and did not exhibit any signs of decomposition or aggregation over a period of several weeks.

The basic strategy for the fabrication of a thiol-functionalized SiO_2 surface using chemical modification approach is presented in Scheme 1;[30] anhydrous toluene (7 mL) was added under an N_2 atmosphere to a Schlenk flask containing 3-μm SiO_2 microspheres (0.53 mg) and then the flask was placed in an oil bath heated at 80 °C. After stirring for 45 min, a solution of MPTMS (0.2 mL) in anhydrous toluene (3 mL) was added dropwise and then the mixture was maintained at 80 °C for an additional 20 h. After centrifuging and removal of the supernatant solution, the particles were washed three times with toluene and EtOH to remove excess MPTMS and then the product thiol-modified SiO_2 microspheres were dried under reduced pressure.

AuNPs were deposited on the surfaces of thiol-modified SiO_2 microspheres through thiol coordination. The solution of thiol-functionalized SiO_2 microspheres (2.8 mg) was added to a solution of AuNPs (20 mL) and stirred for 24 h; the resulting material was centrifuged, washed with DI water, and centrifuged again. Washing was repeated several times. A solution of 1,6-hexanedithiol (0.3 mL) in anhydrous toluene (10 mL) was added dropwise to the colloidal solution of SiO_2@AuNP microspheres and then a solution of AuNPs (20 mL) was added; the resulting mixture was stirred for 24 h and then the contents were centrifuged, washed with DI water, and centrifuged again. This procedure was repeated for several cycles to polymerize the AuNPs in a layer-by-layer manner on the surface of the SiO_2 microspheres. For convenience, the notation SiO_2@AuNP-(number) is applied herein to describe the number of AuNP layers on the surface; for example, SiO_2@AuNP3 and SiO_2@AuNP5 represent the materials obtained after three and five cycles of deposition of the AuNP layers on the surfaces of the SiO_2 microspheres. To enhance the dispersivity, PEG-SH was deposited on the surface of the final AuNP layer. SiO_2@AuNP5 and PEG-SH were mixed at a ratio of 1:1 (1 μmol PEG-SH/1 mg of SiO_2@AuNP) and then the mixture was centrifuged, washed with DI water, and centrifuged again. Washing was repeated several times.

The average crystallite size and crystal structure of the AuNPs on the SiO_2 microspheres were studied using X-ray diffraction (D2 PHASER X-ray Diffractometer, Bruker) with a Cu target radiation (300 W) over a 2θ range from 5 to 80°. Scanning electron microscopy (SEM) images were recorded using a field-emission scanning electron microscope (JSM-6500F, JEOL) operated under a voltage of 15.0 kV. Transmission electron microscopy (TEM) images were recorded using a field-emission transmission electron microscope (Philips Tecnai G2 F20) operated at an accelerating voltage of 200 kV. Specimens for examination under an electron microscope were prepared through evaporation of an anhydrous EtOH solution (one or two drops) of the NPs onto holey carbon films supported on standard Cu grids. UV−Vis and FTIR spectra were recorded using a PerkinElmer lambda 25 spectrophotometer and a Digilab-FTS1000 instrument, respectively.

Polarization of Microspheres under Alternating Electric Fields in an SSD. The SiO_2@AuNP microspheres were dispersed in water at a concentration of 5 wt % to form electrorheological fluids. Electrorheological fluids were also prepared with microsphere concentrations of 1 and 10 wt %, but the microsphere stringing behavior was not obvious under polarization. To observe the polarization of the microspheres, SSDs were fabricated to encapsulate aqueous solutions suspending these microspheres over a large area (Figure 1a). Commercially available ITO glass plates were cleaned sequentially with acetone, isopropyl alcohol, and deionized water. The SU-8 insulating layer was spin-coated (3000 rpm, 30 s) on the bottom ITO-coated glass (ca. 2 μm thickness). Teflon layers were spin-coated (3000 rpm, 30 s) from 1% (w/w) Teflon solution in FC-770 (3M) sequentially on the top and SU-8−coated bottom ITO glass (ca. 50 nm thickness). The top ITO glass plate was coated only with Teflon

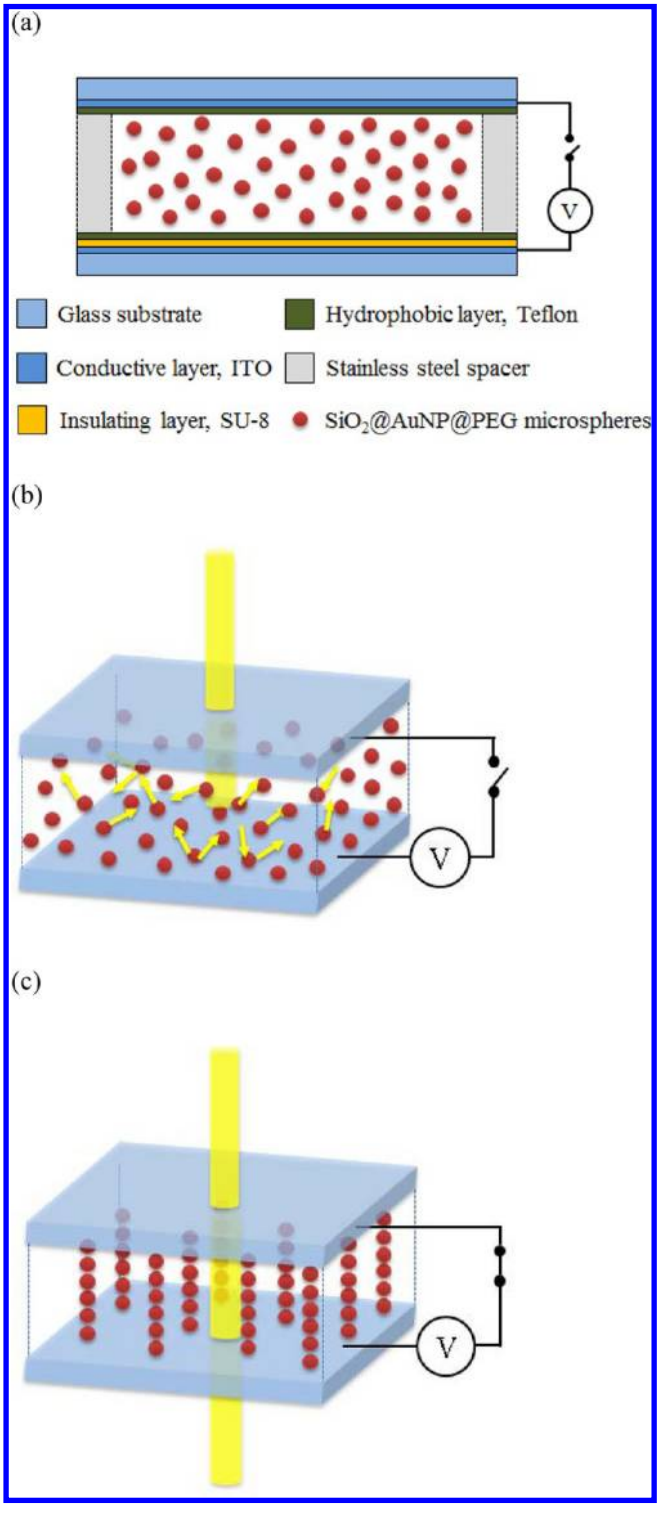

Figure 1. (a) SSD, consisting of a Teflon layer, insulating layer, and spacer coated on two ITO-glasses, operated in (b) dark (microsphere dispersing) and (c) bright states (linear microsphere stringing under polarization).

layer and grounded. Stainless-steel spacer (100 μm thickness) was bonded to the bottom ITO glass using an adhesive. Aqueous dispersions of the microspheres were poured into the region defined by the spacer and the bottom ITO glass. To ensure a precise thickness of the microsphere suspension, the top ITO glass was capped on the spacer with power magnets to form the SSD. The transparent (transmittance: >97% in the visible light range) negative photoresist SU-8 was used as the insulating layer to prevent electrical conduction between the top and bottom ITO glasses. Teflon was used as an extra antiadhesion layer to protect the ITO electrodes. The dielectric constants of SU-8 and Teflon are 3 and 1.93, respectively. A charge-coupled device (CCD) was placed above the SSD to detect the bottom incident light from a halogen lamp. When the incident light was scattered without polarization, a dark state appeared in the CCD image (Figure 1b); when the microspheres were strung linearly along with the electric field, resulting in transmittance of incident light under polarization, a bright state appeared (Figure 1c). A 20-MHz synthesized function generator (Agilent Technologies 33220A) was employed with built-in arbitrary waveform and pulse capabilities. A piezo amplifier (A.A. Lab Systems A-303) was used to amplify the input signal (AC, to 1.5 MHz) to a maximum of 400 V_{P-P}. Using the function generator, the signals of DC or AC electric fields could be applied to the corresponding electrodes. The dynamic image acquisition system comprised an Olympus IX71 inverted microscope, an excitation component, a cooled CCD, and a computer with software. An Ocean Optic USB4000-VIS-NIR spectrometer was used to analyze the SSDs at wavelengths from 350 to 1000 nm; the amplitude of the reflected light was measured using a 3648-element Toshiba CCD array to increase the signal-to-noise ratio; the resolution (full width at half-maximum, fwhm) was approximately 1.5 nm; the integration time was varied between 3.8 ms and 10 s; the sensitivity was 130 photons/count at 400 nm and 60 photons/count at 600 nm. In reflectance measurements, an integrating sphere (diameter: 100 mm) having three openings was set to evenly diffuse the incident light emitted from a 50 W halogen lamp source, which was connected to the side opening of the sphere. The SSD was placed beneath the opening at the bottom of the integrating sphere and the reflected light was recorded vertically by a set of lenses, camera, and spectrometer through the top opening of the integrating sphere, the pinhole, and the waveguide.

For a spherical particle, the variation in the magnitude of the force with frequency is given by the Clausius–Mossotti (CM) factor (f_{CM}). It defines the moment of the equivalent, free-charge, electric dipole that would create a perturbation field identical to and indistinguishable from that of the dielectric sphere for all values of r greater than a.[8] The only distinction between this induced dipole and a general electric dipole is that, because the particle is a sphere and lossless, the moment will always be parallel to the electric field. The force acting on the dielectric spherical particles in a dielectric medium is given by

$$F_{DEP} = (p\nabla)E = \frac{3}{2}\pi\varepsilon_m v f_{CM} \nabla E^2 \quad (1)$$

where $v = 4/3\pi a^3$ is the volume of a spherical particle having a radius a. The real and imaginary parts of the CM factor define both the frequency dependence and direction of the force.

$$p = 4\pi a^3 \varepsilon_m \left(\frac{\tilde{\varepsilon}_p - \tilde{\varepsilon}_m}{\tilde{\varepsilon}_p + 2\tilde{\varepsilon}_m}\right) E \quad (2)$$

The terms in the parentheses, the CM factor (f_{CM}), are frequency-related. In general, the real part of the CM factor is bounded by values of −0.5 and 1; the imaginary part is bounded by values of −0.75 and +0.75.[8] For a homogeneous medium in an electric field, the complex permittivity will have both real (ε') and imaginary (ε'') parts reflecting charge storage in and out of phase, respectively, with the electric field:

$$\tilde{\varepsilon} = \varepsilon_0\left(\varepsilon_{hf} + \frac{\varepsilon_{lf} - \varepsilon_{hf}}{1 + i\omega\tau}\right) - i\frac{\sigma}{\omega} = \varepsilon' - i\varepsilon'' \quad (3)$$

where ε_0 has the value 8.854×10^{-12} Farads/m; ε_{hf} and ε_{lf} are the high- and low-frequency permittivities, respectively; σ is the conductivity of the material, τ is the relaxation time; and ω is the angular frequency of the electric field, equal to $2\pi f$, where f is the frequency of the electric field. In the upper kilohertz to lower megahertz range, the real part is due mainly to the movement of bound charges, whereas the imaginary part arises from the electrical current carried by the mobile charges.[32]

To study of the principle of particle polarization, the factors influencing the particle movement in an electric field were analyzed and compared. First, the force drawing particles to form particle chains was analyzed. Equation 4 expresses the attractive force ($F_{attractive}$) between two induced dipoles.

$$F_{attractive} = \frac{6p^2}{4\pi\varepsilon_m d^4} = \frac{24\pi a^6 \varepsilon_m {f_{CM}}^2 E^2}{d^4} = \frac{24\pi a^6 \varepsilon_m {f_{CM}}^2 V^2}{d^4 D^2} \quad (4)$$

The concentration of particles in solution determines the mean distance between the particles (d). Here, it was assumed that the attractive force was equal to the viscous force, $F_{viscous}$, on a spherical particle at terminal speed. The equation could be expressed as[33]

$$F_{viscous} = 6\pi\eta a v = \frac{6\pi\eta a r}{t} = \frac{24\pi a^6 \varepsilon_m {f_{CM}}^2 V^2}{d^4 D^2} \quad (5)$$

where η, v, and t are the medium viscosity, the velocity of the traveling particle, and the response time, respectively. In addition, for the core/shell structure, the particle complex permittivity $\tilde{\varepsilon}_{cs}$ in the CM factor, f_{CM}, could be expressed as follows:[33]

$$\tilde{\varepsilon}_{cs} = \tilde{\varepsilon}_{external}\left\{\frac{\left[\left(\frac{a_2}{a_1}\right)^3 + 2\left(\frac{\tilde{\varepsilon}_{internal} - \tilde{\varepsilon}_{external}}{\tilde{\varepsilon}_{internal} + 2\tilde{\varepsilon}_{external}}\right)\right]}{\left[\left(\frac{a_2}{a_1}\right)^3 - \left(\frac{\tilde{\varepsilon}_{internal} - \tilde{\varepsilon}_{external}}{\tilde{\varepsilon}_{internal} + 2\tilde{\varepsilon}_{external}}\right)\right]}\right\} \quad (6)$$

where a_2 is the radius of the entire particle (core and shell); a_1 is the radius of the core; and $\tilde{\varepsilon}_{external}$ and $\tilde{\varepsilon}_{internal}$ are the complex permittivities of the shell and core, respectively. In a previous study, particles that were driven by an electric field force in electrophoretic displays were found to travel through the whole thickness of the display medium.[33] The particles in this study were driven by dipole–dipole interactions; they were required only to hide behind the neighboring top particles and traveled much shorter distances than did those in the electrophoretic system. By choosing appropriate concentrations, particle sizes, and device thicknesses, the response speed could become comparable with that of an electrophoretic display (EPD). In situ time response measurements were also performed to confirm the rapid response of the particle polarization; by changing the surface conductivity, the initial response time was only 0.5 ms.[34] Particles featuring a high-dielectric-constant coating can have an enormous electrorheological effect.[35]

RESULTS AND DISCUSSION

Characterization of SiO_2@AuNP Microspheres. Figure 2 presents FTIR spectra of the pure SiO_2 microspheres, thiol-modified SiO_2 microspheres, SiO_2@AuNP, pure PEG-SH, and SiO_2@AuNP5@PEG. The FTIR spectrum of pure SiO_2 microspheres featured strong signals for Si–O–Si stretching at 470, 1095, and 1238 cm^{-1} as well as a peak at 952 cm^{-1} that we attribute to Si–OH bonds.[36] The spectrum of the thiol-modified SiO_2 microspheres exhibited two bands in the ranges 2980–2820 and 2600–2500 cm^{-1}, which we attribute to C–H and S–H stretching, respectively, of the attached thiol groups.[37] After coating these thiol-modified SiO_2 microspheres with AuNPs, the intensities of the signals for the Si–O–Si and Si–OH units decreased significantly, consistent with the presence of shells of AuNP layers on the SiO_2 microspheres. Characteristic absorption peaks for pure PEG-SH appeared at 1110,

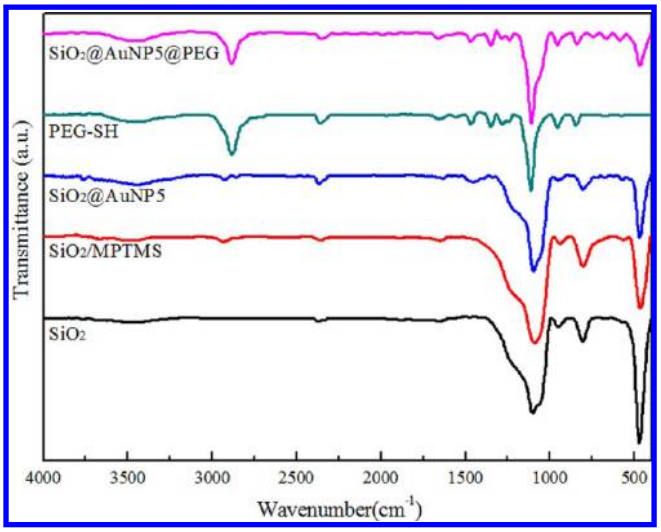

Figure 2. FTIR spectra of bare SiO_2 microspheres, MPTMS-modified SiO_2 microspheres, SiO_2@AuNP5, pure PEG-SH, and SiO_2@AuNP5@PEG.

2885, and 2660 cm^{-1}, associated with stretching vibrations of the C−O−C, CH_2, and S−H groups, respectively.[38] The characteristic bands for SiO_2@AuNP@PEG appeared at 467 (Si−O−Si), 1110 (C−O−C), and 2885 (strong, CH_2) cm^{-1}, confirming the presence of polymer shells on the SiO_2@AuNP particles.[39] Figure 3a displays UV−vis absorption spectra of the colloidal AuNPs (particle size: ca. 6.7 nm), bare SiO_2, SiO_2@AuNP1, SiO_2@AuNP3, SiO_2@AuNP5, and SiO_2@AuNP5@PEG. The surface plasmon resonance (SPR) band in the as-prepared colloidal solution of AuNPs was clearly evident near 525 nm. After assembling the AuNPs through linkers, we expected the interactions between the AuNPs to vary the position of the SPR band in the absorption spectra. In Figure 3a, we observe that the SPR peak red-shifted upon increasing the number of AuNP layers on the microspheres' surfaces, relative to that of the colloidal AuNPs; the maximum red-shift, for SiO_2@AuNP5, was approximately 21 nm. These findings suggest that the colloidal AuNPs gradually covered the surfaces of the SiO_2 cores. Furthermore, grafting the polymer PEG-SH onto SiO_2@AuNP5 resulted in a broader SPR signal.[40,41]

Figure 3b displays XRD patterns that we recorded to investigate the crystallinity of the AuNP shells on the surfaces of the composite microspheres. For the amorphous pristine SiO_2 microspheres, only one broad diffuse peak appeared at a value of 2θ of 23.4°. A weak peak at 37.9° appeared after attaching the first layer of AuNPs. Upon increase the number of AuNP layers, five distinct characteristic peaks appeared gradually at 37.9, 44.2, 64.4, 77.5, and 81.6°, corresponding to the (1 1 1), (2 0 0), (2 2 0), (3 1 1), and (222) lattice planes, respectively, of the face-centered-cubic phase of Au (JCPDS Card No. 89−3697). No external peak appeared for SiO_2@AuNP5@PEG, indicating the amorphous nature of the PEG chains on the surface. The thickness of the assembled AuNP layer on the SiO_2@AuNP5 microspheres was 19.4 nm, calculated from the (111) lattice plane using the Scherrer equation.

Morphology of Core/Shell SiO_2@AuNP Microspheres. Figure 4 reveals the surface topographies of the AuNP-modified SiO_2 microspheres, as observed using SEM. The SiO_2 microspheres had smooth spherical surfaces, with a regular diameter of 3 μm (Figure 4a). A distinctive layer featuring the

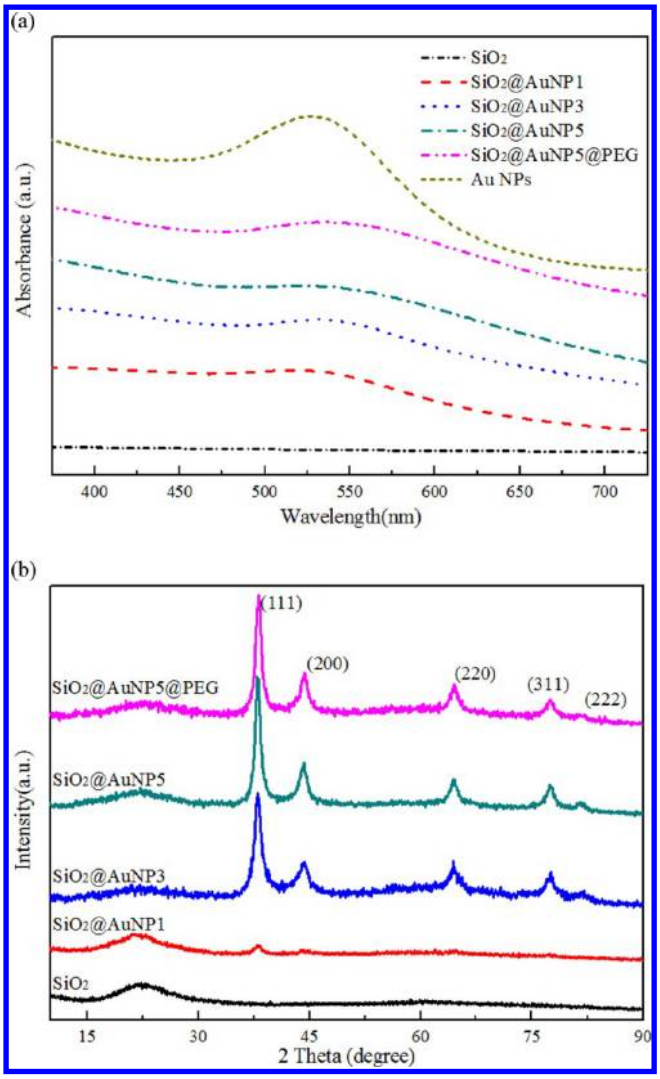

Figure 3. (a) UV−vis spectra of aqueous solutions of colloidal AuNPs (particle size: ca. 6.7 nm), bare SiO_2, SiO_2@AuNP1, SiO_2@AuNP3, SiO_2@AuNP5, and SiO_2@AuNP5@PEG. (b) XRD patterns of bare-SiO_2, SiO_2@AuNP1, SiO_2@AuNP3, SiO_2@AuNP5, and SiO_2@AuNP5@PEG.

elements C (12.74%) and S (1.68%) appeared on the surface of the thiol-modified SiO_2 microspheres after their reaction with MPTMS (Figure 4b). A pebblelike configuration appeared gradually upon increasing the number of poly(AuNP) layers on the surfaces of the microspheres during the formation of the core/shell structures, indicating the gradual increase of the coverage of AuNPs on the microspheres (Figure 4c−e). After grafting PEG-SH onto the poly(AuNP) shells, the roughness of the microspheres' surfaces decreased abruptly, consistent with a covering of soft-matter PEG shells. Figure 5 displays TEM images of these core/shell composite microspheres. A semi-transparent membrane appeared around the SiO_2 microspheres after treatment with MPTMS (Figure 5b). The poly(AuNP) layer formed a shell structure gradually upon increasing the number of layers (Figure 5c−e). The poly(AuNP) layer exhibited slight peeling after five poly(AuNP) layers had been added, possibly a result of the centrifuging processes. We estimated the general size distribution of the nanoshell particles by considering the original SiO_2 core diameter of 3 μm. The shell thicknesses of SiO_2@AuNP1, SiO_2@AuNP3, and SiO_2@

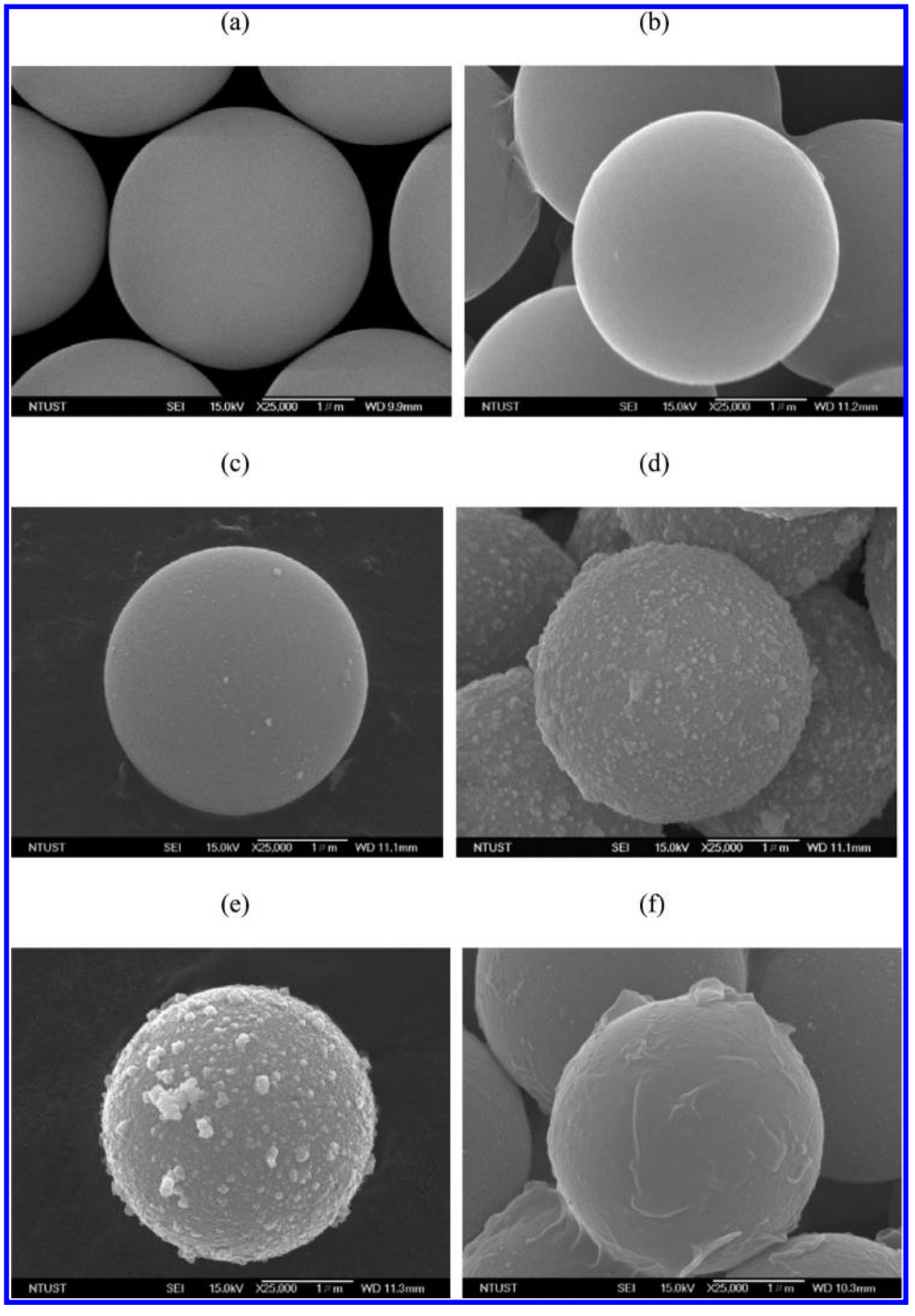

Figure 4. SEM images of (a) bare SiO_2 microspheres, (b) MPTMS-modified SiO_2 microspheres, (c) SiO_2@AuNP1, (d) SiO_2@AuNP3, (e) SiO_2@AuNP5, and (f) SiO_2@AuNP5@PEG.

AuNP5 were 15 ± 5, 25 ± 5, and 40 ± 5 nm, respectively. Thickness of the outermost layer of PEG was approximately 10 ± 5 nm (Figure 5f). Notably, TGA is also a good technique for estimating the shell thicknesses of monodisperse core/shell structured microspheres.[42]

Nanomaterials exhibit remarkable and specific properties, unlike those of their bulk materials, because of their large surface-to-volume ratios, large surface energies, and spatial confinement.[22] For example, single AuNPs and bulk Au behave as insulators and conductors, respectively. Colloidal AuNPs cross-linked to poly(AuNP) undergo a gradual transformation from an insulator to a semiconductor material as a result of a gradual decrease in the average interparticle distance among the AuNPs.[22,30] We evaluated the electro-optical properties (i.e., transmittance) of the microspheres in aqueous solution when encapsulated within SSDs (Figure 1). Figure 6 displays top-view microscopy images, obtained using an inverted microscope, of SSDs encapsulating our microsphere solutions (5 wt %) in the absence and presence of an applied alternating electric field (frequency: 300 kHz; voltage: 50 V). The degree of contrast in the SSD images represents the number of microspheres stringed in a line. For bare SiO_2 microspheres, the SSD remained opaque after applying the voltage, indicating that most of bare SiO_2 microspheres could not be stringed linearly

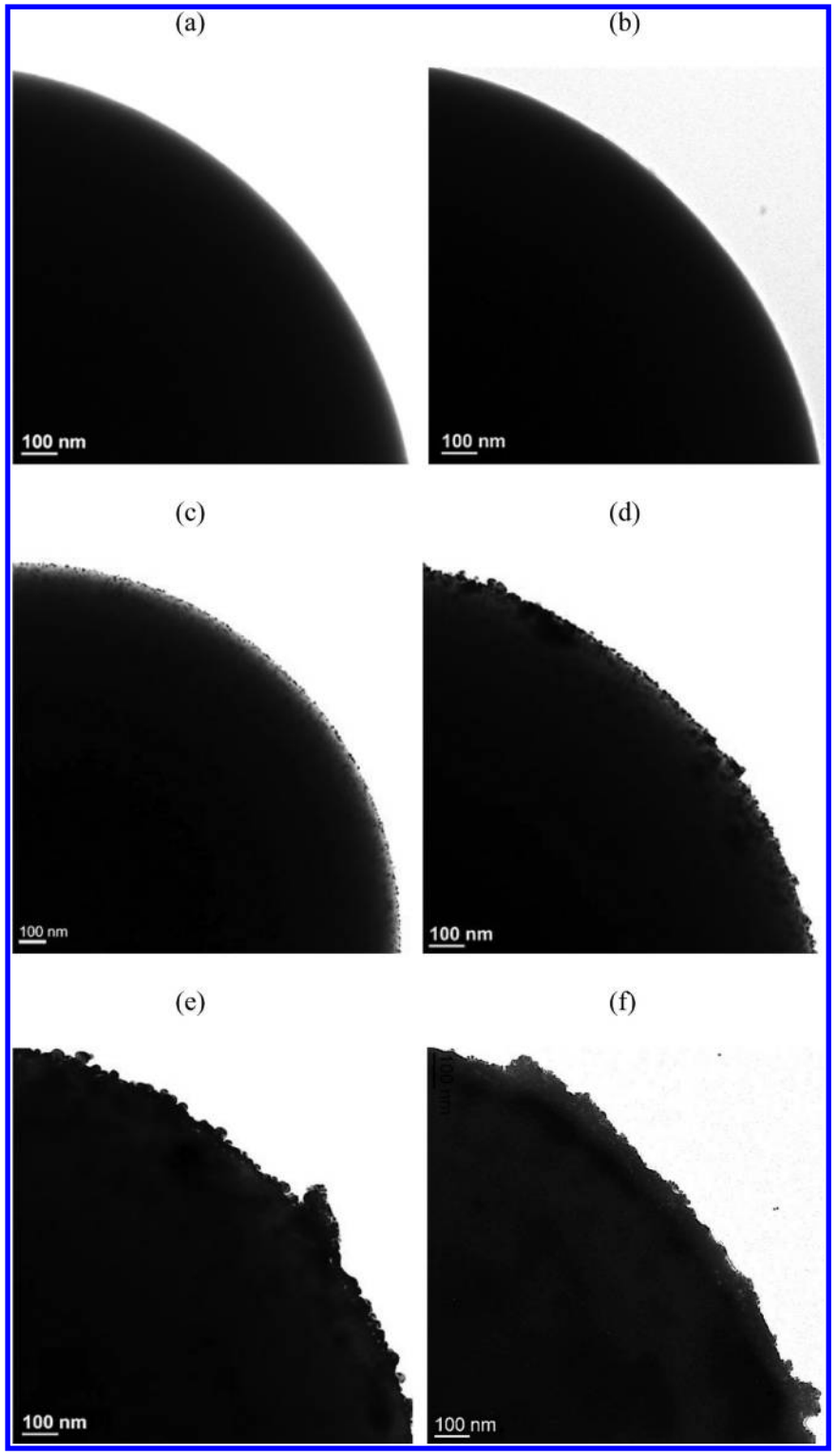

Figure 5. TEM images of (a) bare SiO_2 microspheres, (b) MPTMS-modified SiO_2 microspheres, (c) SiO_2@AuNP1, (d) SiO_2@AuNP3, (e) SiO_2@AuNP5, and (f) SiO_2@AuNP5@PEG.

along the applied electric field (Figure 6a). Stringing the dispersed SiO_2 microspheres in a line (darker microspheres) resulted in higher transmittance of the SSD because of the increase in the light flux area. The darker microspheres displayed in the SSD increased upon increasing the number of AuNP layers, consistent with increased stringing of the microspheres (Figures 6a–d). For SiO_2@AuNP5@PEG in the SSD, most of the microspheres were strung linearly (Figure 6e). The performance of a display would be related to the degree of stringing of the microspheres. We estimated the number of microspheres per area from a top view of the SSD window by an Image-Pro Plus software; the microsphere concentration was controlled in each case at 1.76×10^8 particles/mL. When viewing from the top, the number of bare SiO_2 microspheres was 2400 ± 300 within an area of 175×130 μm^2. The number decreased to 1300 ± 300 after

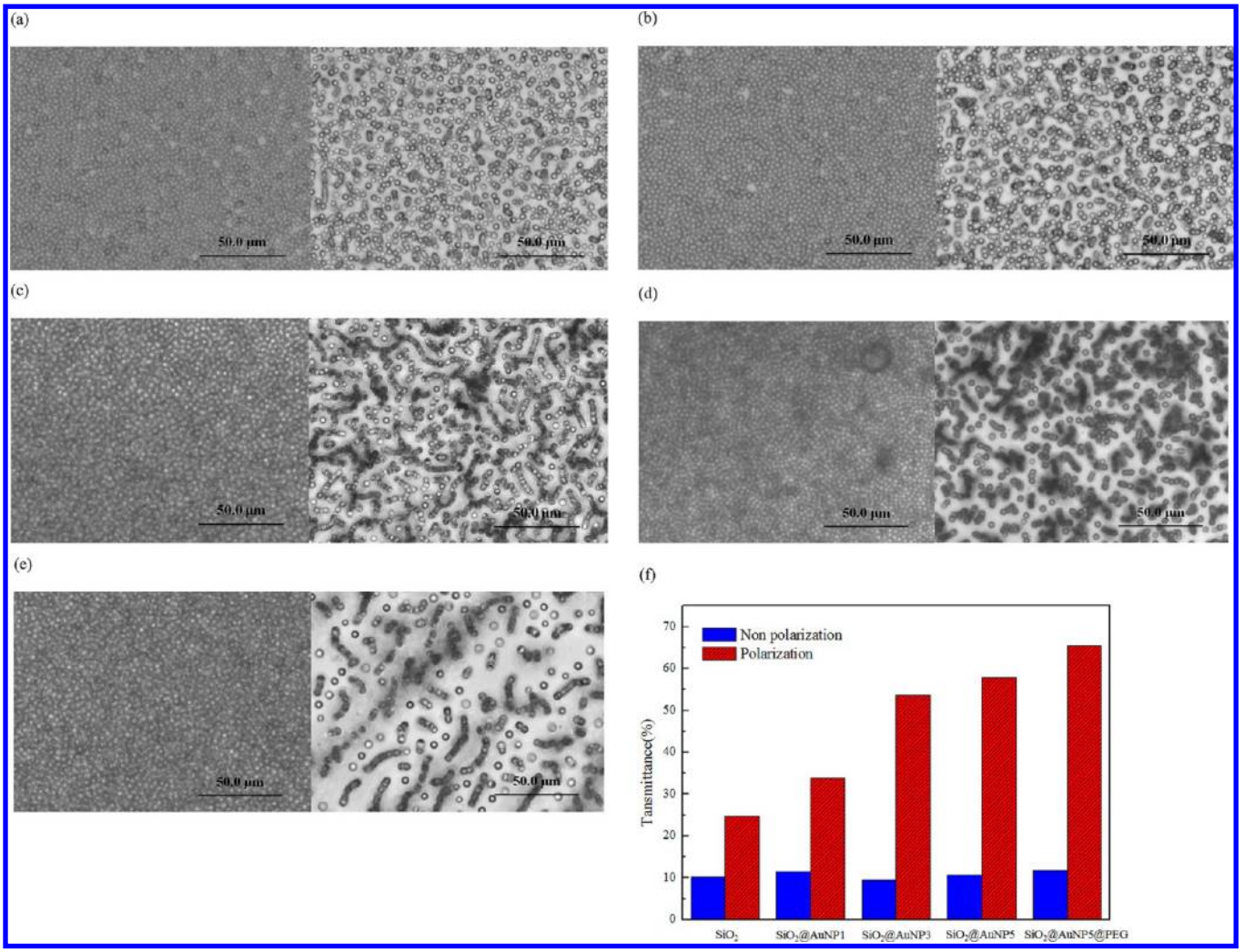

Figure 6. Top-view microscopy images of SSDs encapsulating (a) bare SiO_2 microspheres, (b) SiO_2@AuNP1, (c) SiO_2@AuNP3, (d) SiO_2@AuNP5, and (e)SiO_2@AuNP5@PEG in (left) nonpolarization and (right) polarization states under an alternating electric field (frequency, 300 kHz; voltage, 50 V). (f) Transmittance of SSDs encapsulating bare SiO_2 microspheres, SiO_2@AuNP1, SiO_2@AuNP3, SiO_2@AuNP5, and SiO_2@AuNP5@PEG in nonpolarization and polarization states.

Table 1. Number of the Microspheres, SRs, and OARs Determined from Top Views of the SSDs in Nonpolarization and Polarization States

	no. of microspheres[a]			open area ratio (%)	
sample	nonpolarization	polarization[b]	stringing ratio (%)	nonpolarization	polarization[b]
bare SiO_2	2500 ± 200	1300 ± 200	48.0	3.1	29.3
SiO_2@AuNPl	2400 ± 200	1200 ± 200	50.0	2.8	32.5
SiO_2@AuNP3	2700 ± 200	1000 ± 200	62.9	1.6	52.8
SiO_2@AuNP5	2600 ± 200	800 ± 200	692	1.7	54.2
SiO_2@AuNP5@PEG	2700 ± 200	300 ± 200	88.9	1.4	61.6

[a]Number of the micropheres is counted from top-view images of the display in an area of 175 × 130 μm^2. [b]The alternating electric field at 300 kHz and 50 V of frequency and voltage, respectively, is used to polarize the display.

polarizing, verifying that a substantial degree of stringing of microspheres had occurred (Figure 6a). We define the stringing ratio (SR), representing the degree of linear overlap of the microspheres in the SSD window, as

$$\text{string ratio (SR)} = \left(\frac{N - N_p}{N}\right) \times 100\% \quad (12)$$

where N and N_p represent the number of microspheres counted from top views of the display in nonpolarization and polarization states, respectively. Table 1 summarizes these data. The SR increased gradually upon increasing the number of AuNP layers, suggesting that the presence of poly(AuNP) on the microspheres substantially enhanced the stringing effect in the aqueous solution. The largest SR was that of SiO2@AuNP5@PEG, presumably because the PEG coating enhanced the dispersivity of the microspheres. To precisely evaluate the contrast of the display under nonpolarization and polarization conditions, we calculated the open area ratio (OAR)

$$\text{open area ratio (OAR)} = \left(1 - \frac{A_m}{A}\right) \times 100\% \quad (13)$$

where A and A_m represent the total area of SSD and the isolated strung microspheres from top views, respectively. Table 1 summarizes the OARs of the SSDs at nonpolarization and polarization states. The OAR represents the light flux that could pass through the SSD completely without microsphere blockage. In general, we could not observe the strings of 3 μm microspheres by the naked eye when viewing the SSDs from the top. The OAR decreased slightly upon increasing the number of AuNP layers on the microspheres in the nonpolarization state, indicating that the presence of poly(AuNP) also enhanced the dispersivity in the aqueous solution. The display with the lowest transmittance was that containing SiO_2@AuNP5@PEG, presumably because of its highest dispersivity. The OARs increased abruptly under polarization of these microspheres in aqueous solution. Thus, the presence of poly(AuNP) layers on the microspheres significantly varied the contrast of the SSDs as a result of the stringing of microspheres. In addition, we found that the OAR was related significantly to the transmittance of these SSDs in nonpolarization and polarization states under the alternating electric field (300 kHz, 50 V; Figure 6f). As expected, the SSD encapsulating the SiO_2@AuNP5@PEG solution exhibited the most efficient polarization-respective behavior in term of transmittance; its polarization-respective behavior was reversible for at least 20 cycles. The increase in transmittance upon increasing the number of poly(AuNP) layers under polarization indicates that the dielectric properties of the poly(AuNP) shells varied gradually as a result of the transition of poly(AuNP) from an insulator to a semiconductor.

A microsphere material exhibits polarization-respective stringing behavior at a specific frequency of the alternating electric field for polarization. For polymer microspheres, the stringing behavior occurs optimally under an alternating electric field having a frequency in the range 1−50 kHz.[7] Tuning the frequency of the alternating electric field might potentially lead to the linear stringing of specific microsphere materials to change the display's color in a solution containing a mixture of several kinds of colored microsphere materials. Figure 7a reveals the dependence of the transmittance under an electric field of 50 V upon varying the frequency from 100 to 900 kHz. We observed approximately linear increases in transmittance of the SSDs upon increasing the frequency to 300 kHz, reaching their plateaus between 300 and 900 kHz. Moreover, Figure 7b displays the dependence of transmittance at 300 kHz upon increasing the voltage from 0 to 70 V. For these microspheres, the transmittance of the SSDs increased upon increasing the voltage to 50 V, at which point it reached a plateau, indicating that optimally stabilized microsphere stringing occurred at or above 50 V. A leakage current appeared between the electrodes of the SSD, however, at voltages of greater than 70 V, resulting in the failure of microsphere stringing. Our results suggest that the SiO_2-based microspheres could be stably polarized at 300 kHz and 50 V to undergo stringing, suggesting that the optimal working window for the electric field was in the ranges 300−900 kHz and 50−70 V. In these cases, the poly(AuNP)-modified SiO_2 microspheres exhibited obviously enhanced stringing effects that increased the transmittance of the SSDs. Thus, the frequency and voltage of the applied electric field, as well as the nature of the microsphere material, affected the transmittance of each SSD. In addition, we found that response

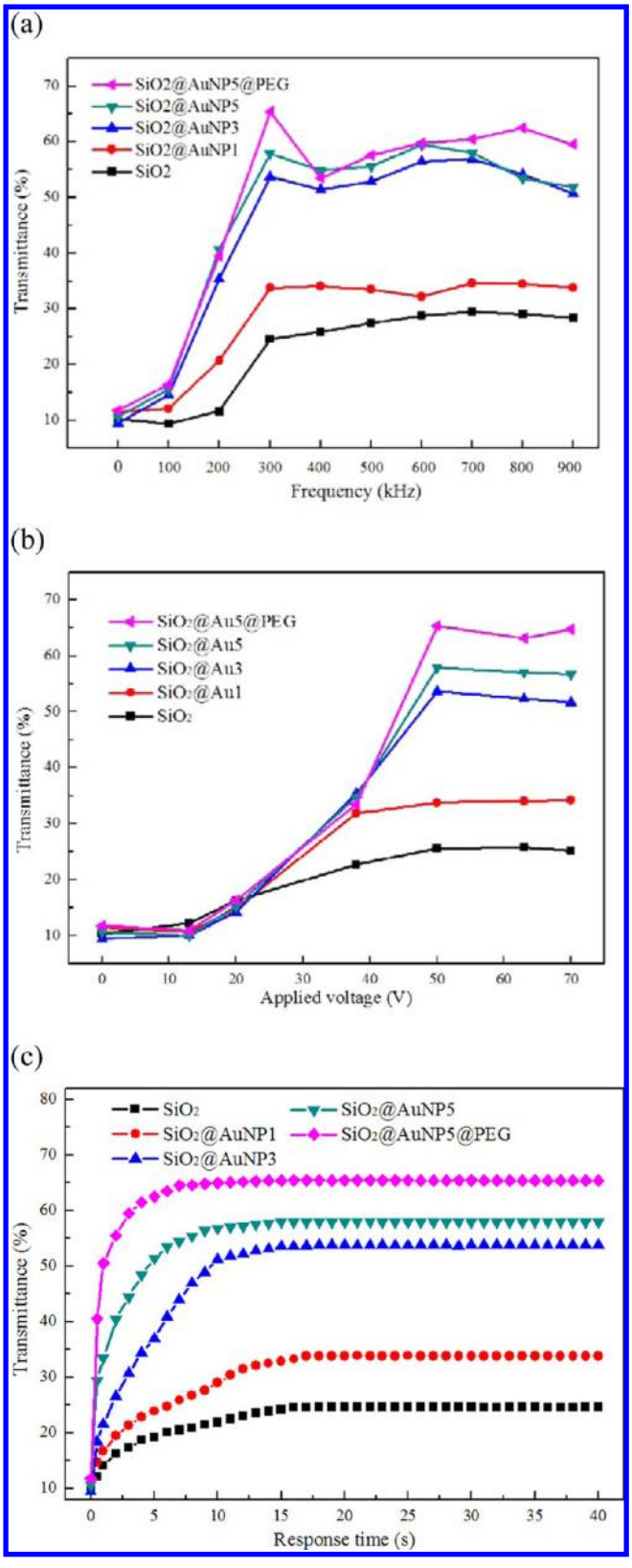

Figure 7. Transmittance of SSDs encapsulating bare SiO_2 microspheres, SiO_2@AuNP1, SiO_2@AuNP3, SiO_2@AuNP5, and SiO_2@AuNP5@PEG under polarization, plotted with respect to the (a) frequency from 100 to 900 kHz at 50 V, (b) voltage from 0 to 70 V at 300 kHz, and (c) response time toward an alternating electric field at 50 V and 300 kHz.

time of the electroresponsive electrorheological fluids was also related to the structure of the poly(AuNP)-modified SiO_2 microspheres (Figure 7c). The highest transmittance of the SSD packed with the bare SiO_2 aqueous solution was achieved after applying the electric field for 17 s. The response time decreased gradually upon increasing the number of layers of the modifying poly(AuNP) on the surfaces of the SiO_2 microspheres. For SiO2@AuNP5@PEG, the microsphere stringing was complete within 8 s.

The real part of the permittivity (ε') is related to the energy stored within the microspheres; the imaginary part of the permittivity (ε'') is related to the dissipation (or loss) of energy within the microspheres. Figure 8 displays the real (ε') and imaginary (ε'') parts of the complex CM function for our microspheres as a function of the frequency. In the range from 300 kHz to 1 MHz, the real part (ε') of the CM function is a predominant factor affecting the dielectrophoretic force among the microspheres, presumably because of movement of the microsphere boundary charges under polarization; in contrast, the imaginary part (ε'') arises from the electrical current carried by the mobile charges. As seen in Figure 8a, the value of ε' decreased abruptly upon decreasing the frequency below 300 kHz. This frequency dependence reflects the fact that polarization of these microsphere does not occur instantaneously in response to the applied field. The results suggest that the polarization response that occurred at frequencies above 300 kHz was always causal (arising after the applied field) and could be represented by a phase difference. For this reason, permittivity is often treated as a complex function (because complex numbers allow specification of magnitude and phase) of the frequency of the applied field. The values of ε' of the CM factors of the SiO_2@AuNP species (Figure 8a) were considerably lower than those of the bare SiO_2. Remarkably, the values of $\acute{\varepsilon}$ were flat across the tested frequency region (from 300 kHz to 1 MHz). Lower permittivity at higher frequencies indicates greater space charge, as has been observed for other metal nanocomposites.[43]

In addition, all of the present SiO_2@AuNP nanocomposites generally exhibited their largest values of ε'' at 100 kHz, suggesting that electrical current carried by the mobile charges was highest at 100 kHz. The values of ε'' clearly increased for samples upon increasing the number of poly(AuNP) layers (Figure 8b). Each sample exhibited a value of ε'' that decreased upon increasing the frequency above 100 kHz, consistent with the behavior of the values of ε'' for these samples, which also exhibited a dependence on frequency at 50 V (see Figure 8a). When thick poly(AuNP) coatings were present on the surfaces of the microspheres, the values of ε' and ε'' at 300 kHz varied because of the semiconducting properties of the cross-linked AuNPs (Figure 8c). The permittivity of a dielectric material decreases with frequency; there is always a delay in the material's response to an applied field, and the material is not completely polarized and relaxed at higher frequencies.

For ideal microsphere stringing, the dielectric losses [$\tan(\varepsilon''/\varepsilon')$] should be as high as possible. Figure 9a reveals that the dielectric losses also followed a similar trend to the values of ε''; that is, it also increased upon increasing the number of poly(AuNP) layers in the samples. Each sample exhibited a dielectric loss that decreased upon increasing the frequency above 100 kHz, consistent with the permittivity (ε'') data for these samples, which revealed a dependence on frequency at 50 V. With a thick poly(AuNP) coating on the surfaces of the microspheres, the losses were significantly enhanced, particularly for SiO_2@AuNP5. The high field loss can be measured in terms of the ratio of energy density recovered and the energy stored. At higher fields (70 V), the dielectric loss was greater than that at low fields (Figure 9b); in addition, the loss increased markedly upon increasing the thickness of the AuNP shells.

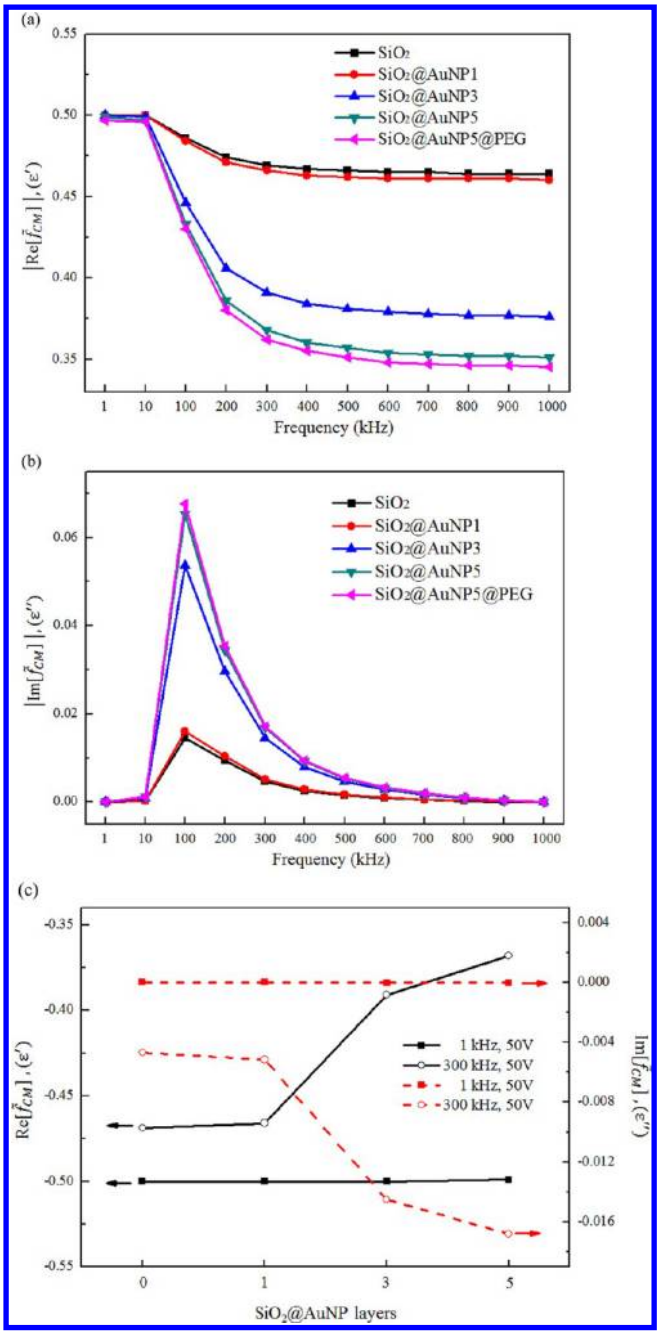

Figure 8. (a) Real (ε') and (b) imaginary (ε'') parts of the dielectric constant of bare SiO_2 microspheres, SiO_2@AuNP1, SiO_2@AuNP3, SiO_2@AuNP5, and SiO_2@AuNP5@PEG, plotted with respect to the frequency (from 100 to 1000 kHz) of the alternating electric field at 50 V. (c) Dependence of the values of ε' and ε'' for the microspheres at 1 and 300 kHz on the poly(AuNP) layer under an alternating electric field of 50 V.

Poly(AuNP) has a large permittivity contrast with the SiO_2 microspheres, which have a permittivity of 3.9. For directly immobilized AuNPs on SiO_2 microspheres, the very large contrast in relative permittivities between host and guest results

dx.doi.org/10.1021/am301543h | ACS Appl. Mater. Interfaces 2012, 4, 5650−5661

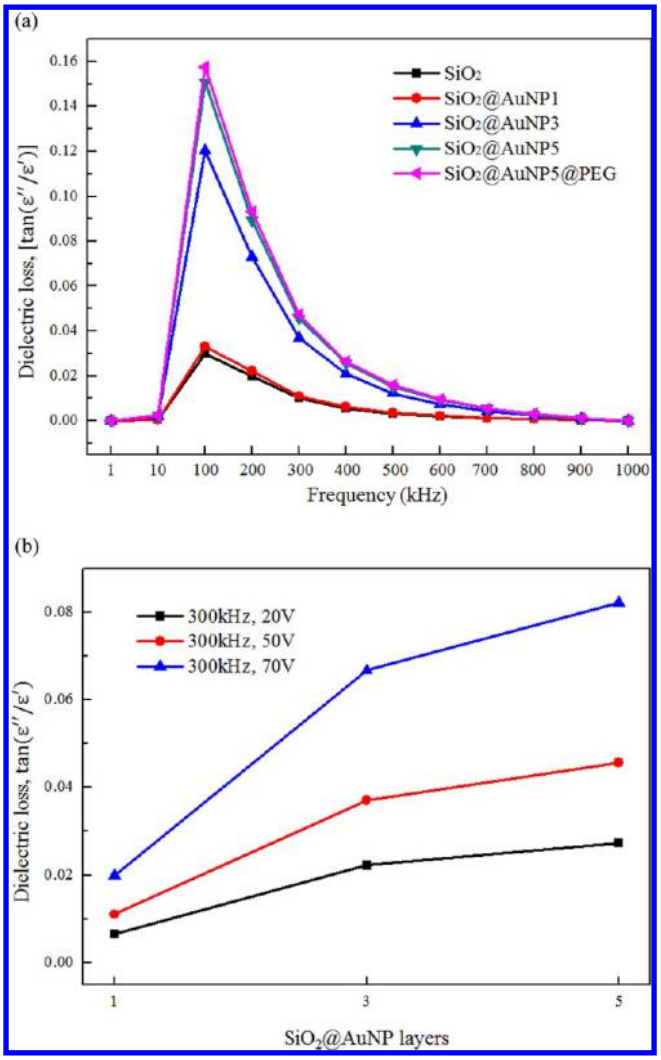

Figure 9. Dielectric loss $[\tan(\varepsilon'/\varepsilon'')]$ of bare SiO_2 microspheres, SiO_2@AuNP1, SiO_2@AuNP3, SiO_2@AuNP5, and SiO_2@AuNP5@PEG, plotted with respect to the (a) frequency from 100 to 1000 kHz at 50 V and (b) number of AuNP layers under an alternating electric field at 300 kHz of 20, 50, or 70 V.

in a large disparity in the electric fields within the constituent phases,[44] inducing discontinuous variations in the local electric field at the interfaces and adversely affecting the bulk dielectric properties. Ideally, composites having graded permittivities, where the permittivity increases gradually from the center of the particle to the border (Figure 10a), should minimize this effect.[38,44] Inclusion of core/shell NPs (Scheme 10b) having a shell permittivity between that of the core and cross-linked AuNPs affords a realistic model to study the effects of permittivity contrast on composite dielectric properties. This approach complements the effects of interfacial layers on laminated semiconductors. For our present materials, the PEG (ε = ca. 13) shell on the NPs acts as a dielectric buffer between the high-permittivity AuNPs and the aqueous solution. With a 10-nm-thick PEG coating on the AuNPs (five layers), we would expect the dielectric loss to decrease because of the high permittivity of the polymer. We found, however, that the dielectric loss increased after coating with PEG, presumably because the PEG coating improved the dispersivity of SiO2@AuNP5. Dielectric loss not only causes dissipation of energy but also produces undesired thermal effects in films. Coating

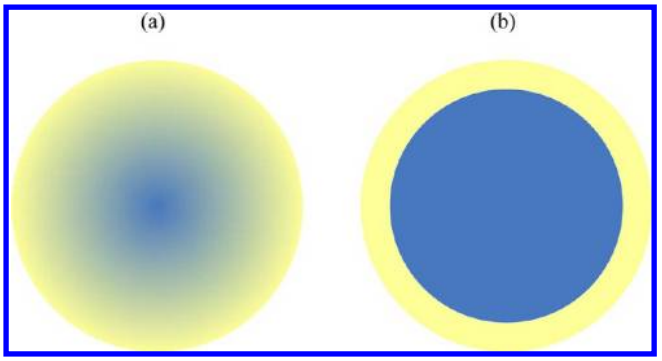

Figure 10. Dielectric composite structural motifs: (a) sphere where the matrix permittivity is graded from the center to the edge and (b) low-permittivity sphere in a high-permittivity matrix.

PEG onto AuNPs inclusions offers an efficient, cost-effective approach to minimizing these adverse effects. We expect that further studies of encapsulated microspheres as fillers in aqueous solution will afford practical routes toward even higher-performing materials for displays.

CONCLUSION

We have developed an effective method for creating AuNP shells on the surfaces of low-ε SiO_2 microspheres in aqueous solution. We used a layer-by-layer approach to self-assemble AuNPs into the form of poly(AuNP) on the surfaces of SiO_2 microspheres; the coating layers were bonded covalently to the surfaces of the microspheres, with their thickness controlled incrementally by varying the number of coating cycles. SSDs encapsulating solutions of poly(AuNP)-modified microspheres exhibited dramatically polarization-switchable transmittances. The reversibility of the polarization-respective behavior was enhanced substantially after AuNP-modification of the SiO_2 microspheres. In addition, we also determined the working widow for the frequency of the electric field for optimal manipulation of the stringing of the microspheres. For a solution containing a mixture of several kinds of colored microsphere materials (e.g., colored PS microspheres), we would expect its SSD to reveal various color images upon manipulating the different microsphere materials through frequency tuning of their stringing states. In addition, we used the complex CM function and the values of ε' and ε'' to determine the dielectrophoretic force for microsphere stringing induced by dipole moments. In situ grafting of PEG (via thiol groups) onto these core/shell microspheres afforded composites with the filler well dispersed in the aqueous solution. The moderate permittivity of the AuNP layer greatly enhanced dielectric loss in these composite materials. Such composites exhibiting efficient linear microsphere stringing behavior are attractive for display applications. We suspect that this approach offers a technology for the feasible realization of electronic paper displays.

AUTHOR INFORMATION

Corresponding Author

*Tel.: +886-2-27376523. Fax: +886-2-27376544. E-mail: jkchen@mail.ntust.edu.tw.

Notes

The authors declare no competing financial interest.

■ ACKNOWLEDGMENTS

We thank the National Science Council of the Republic of China for supporting this research financially.

■ REFERENCES

(1) Hayes, R. A.; Feenstra, B. J. *Nature* **2003**, *425* (6956), 383−385.
(2) Comiskey, B.; Albert, J. D.; Yoshizawa, H.; Jacobson, J. *Nature* **1998**, *394* (6690), 253−255.
(3) Howard, M. E.; Richley, E. A.; Sprague, R.; Sheridon, N. K. *J. Soc. Inf. Display* **1998**, *6* (4), 215−217.
(4) Fan, S.-K.; Chiu, C.-P.; Lin, J.-W. *Appl. Phys. Lett.* **2009**, *94* (16), 164109.
(5) Hashimoto, K.; Okada, M.; Nishiguchi, K.; Masazumi, N.; Yamakawa, E.; Taniguchi, T. *J. Soc. Inf. Display* **1998**, *6* (4), 239−242.
(6) Wang, A.-H.; Hwang, S.-L.; Kuo, H.-T. *Displays* **2012**, *33* (1), 36−41.
(7) Fan, S.-K.; Chiu, C.-P.; Huang, P.-W. *Biomicrofluidics* **2010**, *4* (4), 043011−8.
(8) Chiu, C.-P.; Chiang, T.-J.; Chen, J.-K.; Chang, F.-C.; Ko, F.-H.; Chu, C.-W.; Kuo, S.-W.; Fan, S.-K. *J. Adhes. Sci. Technol.* **2012**, *26*, 1773−1788.
(9) Choi, H. J.; Jhon, M. S. *Soft Matter* **2009**, *5*, 1562−1567.
(10) Liu, Y. D.; Fang, F. F.; Choi, H. J. *Langmuir* **2010**, *26*, 12849−12854.
(11) Jang, I. B.; Sung, J. H.; Choi, H. J. *Synth. Met.* **2005**, *152*, 9−12.
(12) Kalele, S. A.; Ashtaputre, S. S.; Hebalkar, N. Y.; Gosavi, S. W.; Deobagkar, D. N.; Deobagkar, D. D.; Kulkarni, S. K. *Chem. Phys. Lett.* **2005**, *404* (1−3), 136−141.
(13) Leung, S. L.; Li, M.; Li, W. J.; Mai, J. D. *Sens. Actuators, A* **2012**, *178*, 32−39.
(14) Ethiraj, A. S.; Hebalkar, N.; Kulkarni, S. K.; Pasricha, R.; Urban, J.; Dem, C.; Schmitt, M.; Kiefer, W.; Weinhardt, L.; Joshi, S.; Fink, R.; Heske, C.; Kumpf, C.; Umbach, E. *J. Chem. Phys.* **2003**, *118* (19), 8945−8953.
(15) Phonthammachai, N.; Kah, J. C. Y.; Jun, G.; Sheppard, C. J. R.; Olivo, M. C.; Mhaisalkar, S. G.; White, T. J. *Langmuir* **2008**, *24* (9), 5109−5112.
(16) Warshawsky, A.; Upson, D. A. *J. Polym. Sci., Part A: Polym. Chem.* **1989**, *27* (9), 2963−2994.
(17) Wang, W.; Jiang, Y.; Liao, Y.; Tian, M.; Zou, H.; Zhang, L. *J. Colloid Interface Sci.* **2011**, *358* (2), 567−574.
(18) Mayer, A. B. R.; Grebner, W.; Wannemacher, R. *J. Phys. Chem. B* **2000**, *104* (31), 7278−7285.
(19) Kumar, A.; Mandale, A. B.; Sastry, M. *Langmuir* **2000**, *16* (17), 6921−6926.
(20) Shibata, S.; Aoki, K.; Yano, T.; Yamane, M. *J. Sol−Gel Sci. Technol.* **1998**, *11* (3), 279−287.
(21) Xue, J.; Wang, C.; Ma, Z. *Mater. Chem. Phys.* **2007**, *105* (2−3), 419−425.
(22) Chen, J.-K.; Qui, J.-Q. *Colloid Polym. Sci.* **2011**, *289* (17), 1829−1837.
(23) Liang, X.; Xu, Y.; Sun, G.; Wang, L.; Sun, Y.; Qin, X. *Colloids Surf., A* **2009**, *349* (1−3), 61−68.
(24) Chen, J.-K.; Qui, J.-Q.; Fan, S.-K.; Kuo, S.-W.; Ko, F.-H.; Chu, C.-W.; Chang, F.-C. *J. Colloid Interface Sci.* **2012**, *367* (1), 40−48.
(25) Steele, B. C. H.; Heinzel, A. *Nature* **2001**, *414*, 345−352.
(26) Duan, H.; Nie, S. *J. Am. Chem. Soc.* **2007**, *129*, 2412−2413.
(27) Janovák, L.; Dékány, I. *Appl. Surf. Sci.* **2010**, *256*, 2809−2817.
(28) Ulman, A. *Chem. Rev.* **1996**, *96* (4), 1533−1554.
(29) Hasan, M.; Bethell, D.; Brust, M. *J. Am. Chem. Soc.* **2002**, *124* (7), 1132−1133.
(30) Chen, J.-K.; Qui, J.-Q. *J. Nanopart. Res.* **2012**, *14* (6), 1−14.
(31) Brust, M.; Schiffrin, D. J.; Bethell, D.; Kiely, C. J. *Adv. Mater.* **1995**, *7* (9), 795−797.
(32) Valero, A.; Braschler, T.; Renaud, P. *Lab Chip* **2010**, *10* (17), 2216−2225.
(33) Murau, P.; Singer, B. *J. Appl. Phys.* **1978**, *49* (9), 4820−4829.
(34) Wen, W.; Zheng, D. W.; Tu, K. N. *Phys. Rev. E* **1998**, *57* (4), 4516−4519.
(35) Wen, W.; Huang, X.; Yang, S.; Lu, K.; Sheng, P. *Nat. Mater.* **2003**, *2* (11), 727−730.
(36) Biradar, A. V.; Biradar, A. A.; Asefa, T. *Langmuir* **2011**, *27* (23), 14408−14418.
(37) Gao, B.; Chen, Y.; Zhang, Z. *Appl. Surf. Sci.* **2010**, *257* (1), 254−260.
(38) Li, Z.; Fredin, L. A.; Tewari, P.; DiBenedetto, S. A.; Lanagan, M. T.; Ratner, M. A.; Marks, T. J. *Chem. Mater.* **2010**, *22* (18), 5154−5164.
(39) Park, C.; Youn, H.; Kim, H.; Noh, T.; Kook, Y. H.; Oh, E. T.; Park, H. J.; Kim, C. *J. Mater. Chem.* **2009**, *19* (16), 2310−2315.
(40) Feng, L.; Wang, Y.; Wang, N.; Ma, Y. *Polym. Bull.* **2009**, *63* (3), 313−327.
(41) Osterloh, F.; Hiramatsu, H.; Porter, R.; Guo, T. *Langmuir* **2004**, *20* (13), 5553−5558.
(42) Liu, Y. D.; Kim, J. E.; Choi, H. J. *Macromol. Rapid Commun.* **2011**, *32*, 881−886.
(43) Li, Z.; Fredin, L. A.; Tewari, P.; DiBenedetto, S. A.; Lanagan, M. T.; Ratner, M. A.; Marks, T. J. *Chem. Mater.* **2010**, *22* (18), 5154−5164.
(44) Percharroman, C.; Moya, J. S. *Adv. Mater.* **2000**, *12*, 294−297.